Chapter 5

Numerical Simulation and Experimental Testing to Improve Olfactory Drug Delivery with Electric Field Guidance of Charged Particles

Jinxiang Xi and Xiuhua April Si

Additional information is available at the end of the chapter

http://dx.doi.org/ 10.5772/65858

Abstract

Even though the direct nose-to-brain drug delivery has many clinical benefits, there are limited successes in delivering medication aerosols to the olfactory mucosa with standard inhalation devices. In this study, different delivery techniques were assessed in terms of their capacities to deliver drug aerosols to the olfactory epithelium. Specifically, the feasibility of electric field guidance of charged aerosols to the olfactory mucosa was evaluated in an image-based nose model both numerically and experimentally. Multi-sectional nasal cast replicas were fabricated using a 3-D printer to measure the olfactory deposition rates and visualize the deposition distributions. An intranasal deposition test platform was developed that comprised an electric field guidance system, a dry powder charging device, and a point-release nozzle. Numerical simulations were conducted using both ANSYS Fluent and COMSOL. We demonstrated that it is feasible to control charged particles inside the human nose use an external electric field. Both the point-release technique and electric field guidance of drug particles are essential in attaining optimal olfactory doses. Consistent deposition patterns were achieved between in vitro experiments and computational simulations. Future investigations are warrnated for further improvements of olfactory delivery through refining the particle generation, charging, and releasing, and navigation systems.

Keywords: intranasal drug delivery, olfactory region, particle point release, electric field guidance, charged particles, nose-to-brain drug delivery

1. Introduction

Drug delivery for treating neurological disorders such as brain tumors is often forestalled by the blood-brain-barrier (BBB), a network of endothelial cells with tight junctions in the brain's capillaries. The BBB, which can effectively protect the central nervous system (CNS) from pathogens, also prevents therapeutically agents from the diseased tissues in the CNS [1]. For years, the BBB has thwarted the utilizations of many new neurological medications for the treatment of CNS diseases such as brain tumors, depression, and Alzheimer's disease [2, 3].

Intranasal drug delivery to the olfactory epithelium is a noninvasive technique in which medications can bypass the BBB and enter the brain, eliciting a quick uptake and action onset of the therapeutic agents [3, 4]. However, there are many challenges that preclude effective drug delivery to the olfactory region. Very low doses can be delivered to the olfactory region (<1%) via the nasal route using standard nasal devices such as nasal pumps and sprays [5, 6]. It is primarily due to the complicated structure of the human nose, which is composed of convoluted, narrow, and passages. The olfactory mucosa is located at the uppermost part of the nose and is poorly ventilated due to its secluded location [7, 8]. As a result, standard nasal devices have limited success in olfactory drug delivery in that they rely on aerodynamic forces or particle inertia to drive medications to the target area [9]. After administration, particles travel passively with the nasal airflow. Thus, the behavior and fate of these aerosols are primarily dependent on their release positions and initial speeds. Due to the complex nasal structure, most of the medications will be trapped by the nasal valve and turbinate, with very few left that can make their final journey to the olfactory mucosa [10].

Nasal deposition of inhaled aerosols in humans has been extensively investigated both experimentally and numerically. Despite the high variability among subjects, these studies have persistently demonstrated that intranasal drug delivery can be influenced by multiple factors, including patient breathing, nasal devices, administration technique, and drug formulation. Furthermore, local or cellular-level deposition has been shown to be a more appropriate parameter than the total deposition in predicting adverse health effects or therapeutic outcomes. However, reports of local doses are still rare in comparison with extensive reports of total deposition fractions in the literature.

New techniques have been under active investigation to improve the olfactory delivery efficiency. Wang et al. [11] proposed to insert a catheter into the nose and administer drugs beneath the olfactory region. However, due to its invasive nature, this method has the risk to damage the wall tissues when guiding the catheter to the olfactory proximity, and patient compliance is expected to be low. Gizurarson [12] tested a nozzle with a narrow spray angle in hope that aerosols can penetrate into the posterior nose and the olfactory mucosa. A high pressure was necessary for this technique to overcome the nasal resistance so that particles can penetrate into the superior meatus. Hoekman and Ho [13] proposed to use a swirling flow in additional to the narrow spray plume so that particles can penetrate deeper into the upper posterior nose. Persistent higher doses in the olfactory region with swirling flows were measured in rats relative to nonswirling flows. However, extrapolating rat data to humans is

http://dx.doi.org/ 10.5772/65858

difficult because of large interspecies discrepancies [14]. For instance, the olfactory region of a Sprague-Dawley rat covers 45% of the nasal surface, while only 5.2% of the human nasal surface is lined by the olfactory epitheliums in humans [15]. Realizing that a particle released into the nostril at a different location will follow a specific path, Si et al. [6] release drug particles from a selected site in the nostril (termed as point release). Improved dosage in the olfactory region was demonstrated using the point releasing than the traditional whole nostril releasing; however, the improvements are limited and still fall short of the doses to be clinically significant. Considering all the techniques aforementioned, it is noticed that once the particles are released into the nose the particle motions are dictated solely by the aerodynamic force. Due to the complex structure of the nasal structure, most particles will deposit in the nasal valve and turbinate region and only a low percentage of particles penetrate into the olfactory region.

Previous studies have suggested that charged particles under an appropriate electric field can improve nasal and pulmonary drug deliveries [16–18]. Improved dosing of charged particles has been demonstrated in the respiratory tract of both humans and animals [19–29]. Noticing that low olfactory deposition mainly result from the lack of control over particle dynamics in the nose, Xi et al. [25] numerically investigated the transport and deposition of charged particles under different electric strengths and showed that significantly enhanced olfactory dosage is practical by optimizing the electric field strength and particle releasing locations. Similarly, enhanced olfactory dosing can also be attained by using magnetic control of ferromagnetic particles. Preliminary computational simulations predicted a 45.0% deposition fraction for ferromagnetic particles, and the optimal particle diameter is around 15 μm [25].

One issue of intranasal drug delivery of nebulized droplets or small particles is the unwanted dosages into the lungs. One strategy to address this issue is the bi-directional delivery method, which administers medications into one nostril when the patient blows into the apparatus [30]. This method takes advantage of the nature that the soft palate lifts up during exhalation through the mouth, which closes the oropharynx and separates the nasal cavity from the rest of the respiratory tract. As a result, particle penetration into the lungs can be avoided. Moreover, the particles enter one nostril and exit from the other, which allows an increased time for drug deposition. This method did show an increase in medications depositing in the nasal cavity but failed to provide a practical way of dispensing an appreciable amount of medications to the olfactory region [31, 32]. It is hypothesized that by combining the electric guidance of charged particles with the bi-directional strategy, the olfactory dosage can be further enhanced.

The objective of this chapter is to improve the targeted delivery of neurological medications to the olfactory region using both computational modeling and *in vitro* experiments in an image-based nasal airway model. Different strategies were explored to control the intranasal particle motions in order to maximize the dose to the olfactory region and minimize the drug losses in other regions. These strategies include point release, vestibular intubation, deep intubation, and electric guidance of charged particles. Effect of breathing conditions, such as normal inhalation and bi-directional breathing, was also considered.

2. Design of experiments

2.1. Image-based reconstruction of nasal airway model

First, building anatomically accurate airway models is crucial for the assessment of the health outcomes of inhalation therapies. **Figure 1** illustrates the procedures of the translation from medical images into a high-quality computational mesh or *in vitro* casts of the nose-pharynx. To reconstruct the 3-D nasal airway model, MRI scans (512 × 512 pixel resolution) of a healthy 53-year-old male were used. The multislice MRI images were segmented using MIMICS (Materialise, Ann Arbor, MI) to convert the raw image data into a set of cross-sectional contours that define the solid geometry (**Figure 1a**). A surface geometry was reconstructed based on these contours in Gambit (Ansys, Inc.). This surface geometry as shown in **Figure 1b** was subsequently imported into ANSYS ICEM (Ansys, Inc.) for meshing. In general, unless for extremely high-quality image data, a solid model that is directly reconstructed from medical images cannot be used for computational meshing due to the artifacts and resolution limits inherent in current imaging techniques. Considering the high complexity of the nasal airway structure, an unstructured mesh was generated with fine boy-fitted cells in the near-wall region (**Figure 1c**). This nasal geometry has been reconstructed with minimal surface smoothing and was intended to accurately represent the nasal anatomy of human adults. More details of image-based model development can be viewed in a recent video article from our group [33]. This model was also manufactured into hollow casts for *in vitro* studies using 3-D prototyping techniques (**Figure 1d**).

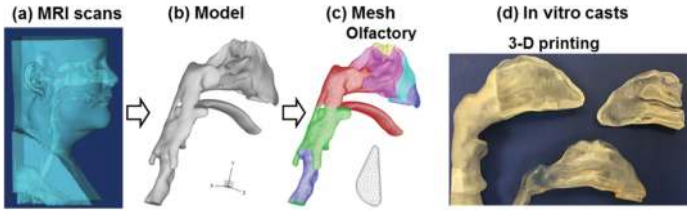

Figure 1. Procedures of translating medical images into computational mesh and *in vitro* casts. First, MRI scans were segmented to reconstruct the airway surface model. Second, high-quality computational mesh was generated with fine near-wall cells. Hollow *in vitro* cast replicas were also fabricated using 3-D printing technique and were used for experimental deposition studies. In order to study deposition distributions, the nasal cavity was divided into different regions: vestibule-valve region (VV), turbinate region (TR), nasopharynx (NP), and olfactory region (OL) that was at the very top of the nasal cavity (yellow color in middle panel).

2.2. Computational fluid-particle transport models

2.2.1. Airflow and particle dynamics

Depending on breathing activities, multiple flow regimes, such as laminar, transitional, or fully turbulent, can exist in the human respiratory tract. The two-order turbulence models have been shown to adequately capture the main flow features and particle transport if a fine body-fitted

http://dx.doi.org/ 10.5772/65858

mesh is used near the wall [34]. In particular, the low Reynolds number (LRN) k-ω model has been widely adopted in computational studies of respiratory flows. It has been validated in many studies to be able to accurately predict the particle transport and deposition in the oral airway [35, 36], nasal cavity [8], and lungs [37, 38]. Moreover, the LRN k-ω model was demonstrated to accurately predict the flow regime transition when the turbulent viscosity approaches zero [39]. Governing equations for the turbulent kinetic energy (k) and dissipation rate (ω) can be found in Wilcox [39].

Transport of monodisperse aerosols was solved using the discrete Lagrangian tracking algorithm through the integration of the particle dynamic equation. Spherical shape was assumed for each particle. The particle diameters range from 0.2 to 5 μm, which have very low Stokes numbers ($St_k = \rho_p d_p^2 UC_c/18\mu D_h << 1$), with ρ_p being the density of the particles (1.0 g/cm^3), U being the fluid velocity, C_c being the Cunningham slip factor [40], and D_h being the nostril effective diameter. The governing equation of Lagrangian tracking is

$$\frac{dv_i}{dt} = \frac{f}{\tau_p C_c}\left(u_i - v_i\right) + g_i\left(1-\alpha\right) + f_{i,Brownian} + f_{i,lift} + f_{i,electric} \tag{1}$$

where u_i is the airflow velocity, v_i is the particle speed, f is the drag coefficient, and $\tau_p = \rho_p d_p^2/18\mu$ is the particle characteristic time to respond to flow variations. The drag coefficient f was based on the equation of Morsi and Alexander [41]. Gravity and Saffman lift force were also included for particles >1 μm [42]. Brownian motion effects were included for submicron particles [35]. It was assumed that particle motion had no effect on the flow field, i.e., a one-way coupling between fluid and aerosols in light of the dilute concentration of pharmaceutical aerosols. The impact of the anisotropic flow fluctuations near the wall was also included by applying an anisotropic turbulence model as described by Matida et al. [43]:

$$u'_n = f_v \xi \sqrt{2k/3} \quad \text{and} \quad f_v = 1 - exp(-0.002y^+) \tag{2}$$

In the above equation, f_v is a damping component normal to the airway wall and ξ is a random number generated by the Gaussian probability density function.

2.2.2. Electric field and electric force

For the direct current (DC) field, the electric potential, U_{DC}, is attained by solving the Poisson's equation,

$$-\nabla \cdot \varepsilon_0 \varepsilon_r \nabla U = 0 \tag{3}$$

where ε_0 and ε_r are the absolute (F/m) and (dimensionless) permittivity of the free space, respectively. The zero value on the right-hand side of the equation means no space charge. For

the alternating current (AC) field, the AC potential is computed by solving the conservation of electric currents [44]:

$$-\nabla \cdot \left(\sigma + j\omega\varepsilon_0\varepsilon_r\right)\nabla V = 0 \tag{4}$$

In the above equation, σ is the electrical conductivity and ω is the alternating frequency (Hz). Considering that the equations for both DC and AC fields are linear, the total electric field can be obtained by superposing the DC and AC fields.

The electric force as a function of the electric field can be expressed as

$$f_{i,electrophoretic} = neE = ne\left(E_{DC} + E_{AC}\right) \tag{5}$$

where n is the nondimensional charge number and e is the elementary charge (e = 1.6 × 10^{-19} C). E_{DC} and E_{AC} are the intensity of the DC and AC electric fields, respectively, which are calculated as follows:

$$E_{DC} = -\nabla U;\ E_{AC} = -real[\nabla \tilde{V} e^{(j\omega t)}] \tag{6}$$

The symbol $\tilde{V}$ means that the AC potential is a complex variable.

2.2.3. Numerical methods

To solve the concomitant flow-electric-particle multiphysics involved in each of the cases considered, ANSYS Fluent (Canonsburg, PA) and COMSOL (Burlington, MA) were employed to simulate the airflow, electric field, and particle tracing. User-supplied functions (UDFs) in the language of Fortran ad C were developed for the calculation of mass flux to the wall, initial particle profile, Brownian force [45], near-wall velocity interpolation [36], and anisotropic turbulence effect [43]. Body-fitted computational mesh was generated to resolve the large gradients of flow velocities near the airway surface. Local mesh refinement was made considering the complex anatomy of the nasal cavity. A grid independence study was performed by evaluating various grid densities, such as 0.4, 0.8, 1.2, and 2.2 million computational cells. The variation in predicted deposition fraction was 1% or less when changing the grid density from 1.2 to 2.4 million. Therefore, the computational mesh of 1.2 million cells was implemented for all subsequent simulations.

2.3. Experimental setup and materials

2.3.1. In vitro test platform

The *in vitro* test platform for intranasal delivery of charged particles has four components: a particle charging apparatus (**Figure 2a**), a three-dimensional replica of a normal human nasal

http://dx.doi.org/ 10.5772/65858

cavity, voltage supplies to induce electric fields, and a scale to quantify deposition. A powder coating system (Powder System Solutions, Nolensville, TN) was modified to charge the dry powders. Copper plates and DC power supplies (MPJA, Lake Park, FL) were implemented to produce external electric fields. A high-precision electronic scale (Sartorius) was utilized to quantify the deposited mass of aerosols. A microscope (AmScope B120C-E1) was used to estimate the diameter of the charged particles. Details of the sectional nasal cast preparation and experimental procedures are described below.

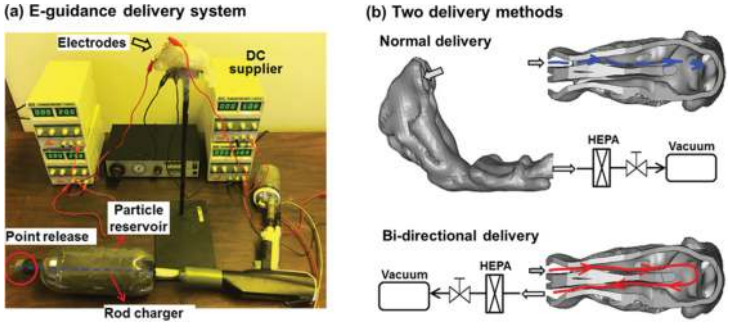

Figure 2. *In vitro* experiments to test the feasibility of electric-guided olfactory drug delivery: (a) experimental setup and (b) two delivery strategies: normal and bi-directional. In both delivery strategies, drug particles are administered into the right-side nostril. However, particles exit the airway through the trachea in the normal delivery and exit through the left nostril in the bi-directional delivery.

2.3.2. Multisectional nasal cast

A multisectional nasal replica was prepared that allows quantitative measurement of regional deposition as well as direct visualization of deposition distributions. After developing the nasal airway geometry model as listed in 2.1, Magics (Materialise, Ann Arbor, MI) was utilized to create the nasal cast wall with a constant layer of 4 mm. The nasal replica was divided into several parts: the nasal vestibule and valve, turbinate, and nasopharynx, as shown in **Figure 1b**. Step-shaped grooves were created at the ends of each replica section for proper sealing and easy assembly. To visualize deposition distributions within the nasal cavity, the nasal replica was cut open along the top ridge of the right nasal passage to disclose the septum and turbinate in the right nose. In order to characterize the olfactory doses, the section representing the olfactory mucosa was separated from the other region. An in-house 3-D printer with a resolution of 16 μm (0.0006 in) (Stratasys Objet30 Pro, Northville, MI) was utilized to fabricate the nasal casts using polypropylene (Veroclear, Northville, MI) that has a clear color and allows for a smooth surface.

2.3.3. Experimental procedures

Dry powders of 30 μm in size (matte black powder coat paint) were selected in this study for their easy availability and excellent charging properties. and easy ava. The modification made

to the powder coating system integrated a charging reservoir (a 2-L bottle) to the nozzle of the charging gun (**Figure 2a**). An additional metal wire was added to extend the charging rod to the reservoir exit, with the wire's length being parallel with the direction of the flow of solid particles. A high voltage supply (Spectracoat coating system), which has an adjustable potential output of 0–100 kV, was connected to the rod. The solid particles were distributed out of a 4-mm-diameter nozzle and subsequently distributed into a multisectional nasal cast replica. Three copper-plated electrodes (A, B, C) were attached to the top of the nose replica, and one copper-plated electrode (D) was attached to the bottom of the replica. Charged dry powders were distributed from the powder coat gun for 20 seconds per trial. For the normal delivery, particles were administered into one nostril and exited through the nasopharynx (**Figure 2b**, upper panel). In contrast, for the bi-directional delivery, the bottom of the pharynx was blocked to simulate the uplifted soft palate, while particles were administered into one nostril and exited through the other (**Figure 2b**, lower panel). A vacuum pump (Robinair 3 CFM, Warren, MI) was connected to the exit of the nasal replica in each test case to simulate the respiration. An in-line flow meter (Omega, FL-510, Stamford, CT) was used to monitor the volumetric flow rate.

2.3.4. Statistical analysis

The variable of interest in this study was the ratio of the olfactory dosage to the vestibule-turbinate dosage (i.e., olfactory-nasal dosage ratio). Results were represented as the main ± standard deviation (SD), with SD being calculated from five trials for each scenario. Statistical analysis software Minitab (State College, PA) was applied to analyze the deposition data. Tukey's method and analysis of variance (ANOVA) were implemented to assess the data variances. The difference was considered statistically significant if the p-value was <0.05.

3. Results

3.1. Numerical (ANSYS Fluent) assessment of olfactory delivery with nasal intubations

Figure 3a shows the motion of 1 μm particles inside the nasal airway predicted using ANSYS Fluent. It is observed that particles that are released from the tip of the nostril move along the upper nasal cavity, while particles from the base of the nostril move along the nasal floor. At an inhalation rate of 20 L/min (normal breathing condition), it takes around 0.02–0.03 seconds for the particles to be delivered to the olfactory region after administration (**Figure 3a**). Faster movements of particles are noted in the middle passages and slow-moving aerosols are observed in the near-wall region. The numerical model in this study had been validated by comparing to *in vitro* deposition data measured in a comparable nasal replica. Good agreement was obtained between the numerically predicted and *in vitro* measurements in comparable nasal casts by Cheng et al. [46, 47] (**Figure 3b**). It is emphasized that the computational nasal airway model in this study and the *in vitro* nasal casts in Cheng et al. [46] were reconstructed from the same set of MRI images.

http://dx.doi.org/ 10.5772/65858

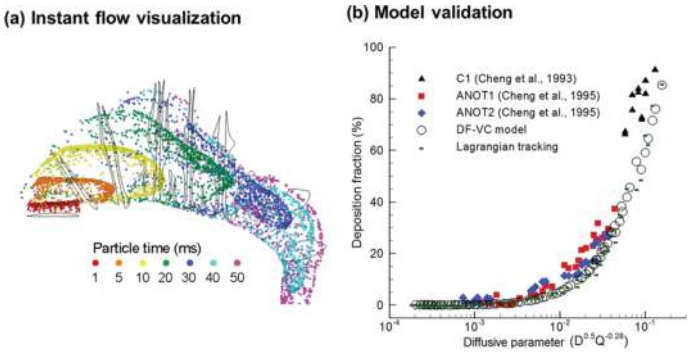

Figure 3. Nasal particle motion and model validation. (a) Snapshots of particle motion at varying instants. (b) Good agreement in nasal deposition between the numerical predictions and experimental measurements of Cheng et al. [46, 47].

In this study, we first tested the feasibility of optimizing particle release positions (smart delivery concept) for intranasal olfactory drug delivery. Two protocols were tested, with the first termed as "vestibular intubation" where particles are released from a selective point in the vestibule (**Figure 4a**), while the second protocol being the "deep intubation" with the nebulizer nozzle inserted directly below the olfactory mucosa (**Figure 4a**). In principle, particles released into the upper vestibule moves along the upper nasal passage and therefore are more likely to deposit in the olfactory region. The computational simulations also confirm that it can deliver higher doses to the olfactory region for both particle sizes considered (150 nm and 1 μm). Furthermore, the deposition pattern appears to be focused close to the olfactory region. Considering the deep intubation protocol, the nozzle was inserted right below the olfactory mucosa so that filtration by the nasal valve and turbinate can be avoided. Therefore, elevated doses were predicted in the olfactory proximity with nonsignificant doses in the middle and inferior turbinate regions.

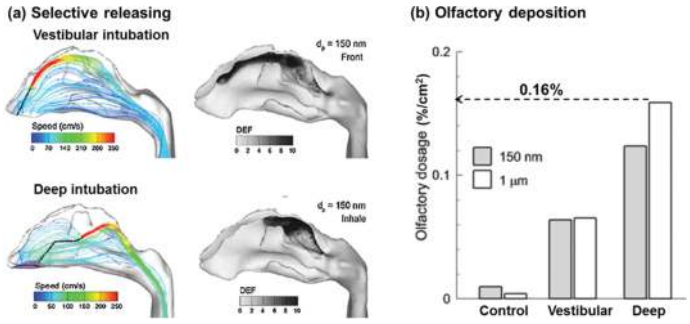

Figure 4. Two delivery protocols with selective particle releasing: vestibular intubation and deep intubation. (a) Streamlines and surface deposition. (b) Olfactory deposition rate with the vestibular and deep intubations in comparison to the conventional delivery method, which releases drugs to the entire nostril (control case).

The olfactory doses between the vestibular and deep intubation protocols, as well as the conventional delivery method, were compared on the basis of deposition fraction per area (%/cm^2) (**Figure 4b**). The surface area of the olfactory mucosa in this study (**Figure 1c**) is 6.8 cm^2. Overall speaking, both intubation protocols significantly enhanced the olfactory targeting while the deep intubation outperformed the vestibular intubation. However, it is noted that even using the deep intubation method, very low fractions of administered dose (0.16%/cm^2 or 1.09% in the olfactory region) were delivered to target, while nearly 99% was lost in other regions, causing tremendous waste and potentially significant unwanted side effects. Therefore, further efforts are needed to explore strategies that can precisely target drug particles to the olfactory region while minimizing drug loss to other tissues.

3.2. Sar-Gel visualization of nasal deposition distributions

Sar-Gel visualization of the local deposition inside the nasal replica is displayed in **Figure 5** for two common nasal spray products (Astelin and Nasonex). The angle of the spray plume was approximately 35^o ± 0.8^o for Astelin and 20^o ± 0.5^o for Nasonex. The majority of spray droplets were trapped by the narrow flow-limiting nasal valve. It is noted that the drug distribution is largely dictated by the physical properties of spray droplets. The high filtration by the slit-shaped nasal valve can be attributed to the high inertia of spray droplets that have large sizes (70–90 μm) and exit from the spray pumps with relatively high speeds. Dripping was absent in Astelin that had a wide spray plume angle, while dripping was observed in Nasonex that had a narrow plume and was prone to cause local droplet accumulation (**Figure 5a** vs. **5b**). Deposition of Astelin appeared to be more dispersed than Nasonex.

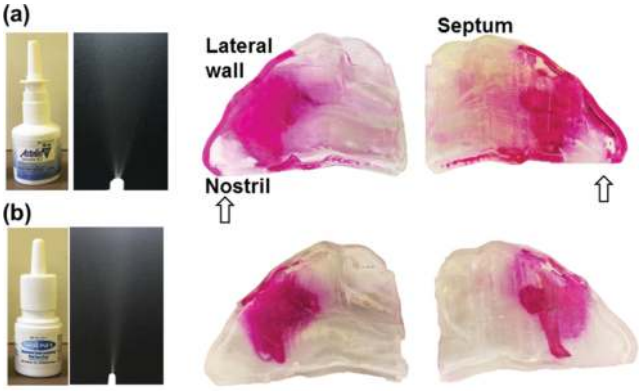

Figure 5. Deposition pattern in the nose with two nasal spray products: (a) Astelin and (b) Nasonex. The majority of spray droplets deposit in the nasal vestibule and valve region and cannot reach the olfactory region.

A commercially available jet nebulizer (Philips Respironics InnoSpire) was utilized to evaluate particle deposition in the nose. Nebulized aerosols were released into the nostril at an orientation 15^o from the vertical direction. As shown in **Figure 6**, most administered droplets deposited in the anterior nose (vestibule and valve regions). Aerosol deposition in the middle

http://dx.doi.org/ 10.5772/65858

and inferior turbinate was also observed, but at a lower level than the anterior nose. Almost no aerosol deposited in the superior meatus and olfactory region (dashed blue ellipse). The above deposition distribution is similar as that reported in Laube [48] who observed predominant doses in the anterior nose. Both **Figures 5** and **6** corroborate the observation that conventional nasal devices cannot deliver adequate doses to the olfactory mucosa, and thus advanced drug delivery systems are warranted in order to achieve clinical significant olfactory delivery.

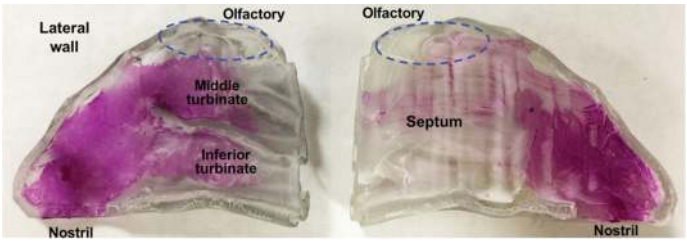

Figure 6. Sar-Gel visualization of the nasal deposition pattern using a standard nebulizer. Even though some nebulized aerosols escape the nasal valve filtration, most of them deposit in the turbinate region and only a very small fraction reaches the olfactory region.

3.3. Multiphysics (COMOL) simulations of olfactory dosing delivery of charged particles

3.3.1. Electric-guided olfactory delivery diagram

The principle of olfactory drug delivery under electric guidance is illustrated in **Figure 7**. There are four essential functions in this device: (1) generation, (2) charging, (3) focusing, and (4) navigation of the pharmaceutical aerosols (**Figure 7a**). A head brace can be added to fix the device relative to the patient's head. Commercially available nebulizers (droplets) and dry powder inhalers can be used to generate aerosolized particles [49]. Particle charging was achieved by letting particles going through a charging chamber, and the acquired charge number can be controlled by varying the voltage supply to the charging chamber [50]. The focusing chamber is composed of several slits [51], with the first slit having a positive voltage and the last one having zero voltage. When the positively charged dry powders travel through these slits, a repulsive force from the slit pushes the dry powders inward to form a focused beam; simultaneously, the forward component of the repulsion accelerates the aerosol beam to a certain exiting velocity. The benefit of knowing the initial speed of particles is that the deposition pattern can be estimated beforehand so that the optimal delivery protocol can be selected. Another benefit is that drug delivery will be more independent of the breathing condition if the initial particle velocities are much higher than the respiratory airflow velocities. This feature is very desirable for inhalation therapy for seniors or people with breathing problems or low compliance capability. After particles were administered into the nose, they will experience an external electric force and divert from their original course. For optimal drug delivery to the olfactory region, particles should move along the middle passage of the

nose to minimize wall losses (**Figure 7b**). In this chapter, we will evaluate whether it is feasible to enhance the olfactory doing through electric guidance of charged particles with charge levels and electric potentials that are safe to humans.

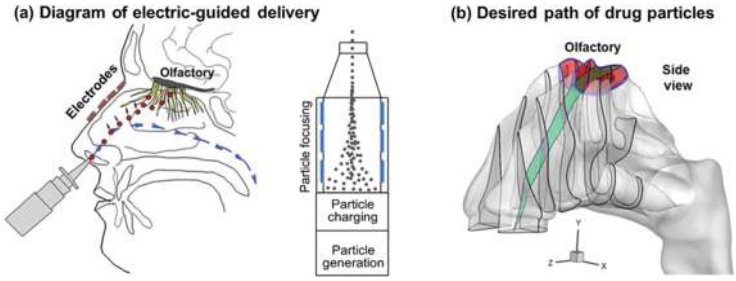

Figure 7. Diagram of electric-guided olfactory drug delivery. (a) Charged particles will be attracted toward the olfactory region by an applied electric field. (b) For optimal olfactory drug delivery, particles should travel along the middle plane of the nasal passage.

3.3.2. Idealized 2-D nose model

The proposed delivery protocol was first evaluated in an idealized 2-D nose configuration. The inhaled airflow field in the nose is shown in **Figure 8a**. There are three streams due to the obstruction of the inferior and middle turbinate. The upper flow stream is further divided by the superior turbinate. Only a small fraction of inhaled airflow was ventilated into the uppermost olfactory region. Due to poor olfactory ventilations, inhaled particles are unlikely to be conveyed to the olfactory region by convection or inertia. It is also observed in **Figure 8a** that stream traces initiating from the posterior naris move toward the nasal floor, while those from the anterior naris move toward the upper passage (superior meatus). It is hypothesized that pharmaceutical agents released into the at the naris tip have a larger chance to deposit into the olfactory mucosa.

To generate a desirable external electric field, four electrodes were put on top of the nose. The electrode voltages were specified to be −3, −8, −12, and 0 V, respectively (**Figure 8a**). The small electric potential (3 V) above the nasal vestibule was intended to impart particles an upward attraction. The electric potential above the middle nose was increased to −8 V to attract particles further toward the olfactory mucosa. The electric potential close to the olfactory region was around −12 V in order to catch the charged aerosols. **Figure 8b** shows the numerically predicted electric field (E-field), which changes from nearly 0 V at the nostrils to about −12 V at the olfactory region.

From **Figure 8c**, electric guidance of charged particles significantly increased the olfactory dosing, which was two orders of magnitude higher in comparison with that when an electric field was absent. **Figure 8d** displays particle transport in the nose 1 second after administration. The majority of particles (∼95%) deposit in the olfactory mucosa. As a comparison, only 0.77% deposit in the olfactory region without an electric field.

http://dx.doi.org/ 10.5772/65858

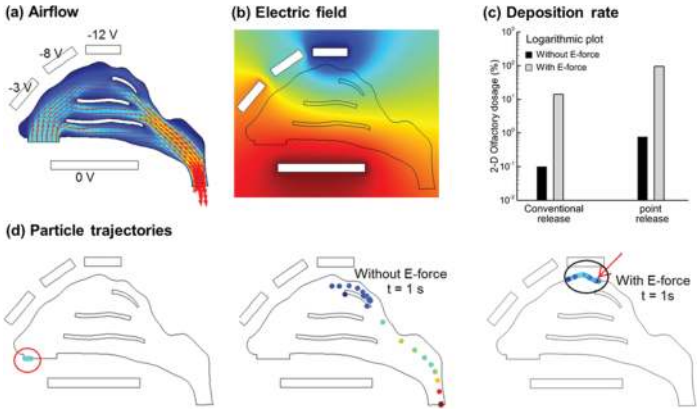

Figure 8. Computational modeling of electric-guided delivery in a 2-D nose model. (a) Airflow field, (b) electric field, (c) comparison of the olfactory deposition rates with and without electric guidance for conventional and point-release delivery techniques, and (d) particle trajectories with and without electric force for the point-release technique. Electric-guided delivery of charged particles can enhance the olfactory doses by two orders of magnitude relative to the case without an electric field.

3.3.3. Realistic 3-D nose model

A comparison of deposition patterns in the image-based 3-D nose model with and without electric guidance is shown in **Figure 9a**. The charge number of the particles is 5000, and the particle size is 0.5 μm. With an appropriate electric field, 3.7% of inhaled particles reached the olfactory mucosa (**Figure 9a**). However, only 0.06% of administered aerosols delivered to the olfactory mucosa without electric guidance.

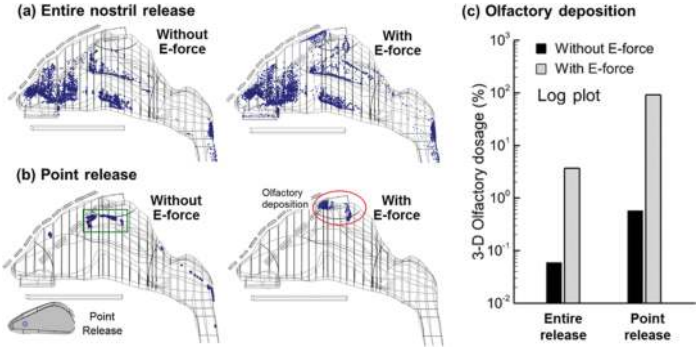

Figure 9. Computational modeling of electric-guided delivery in an anatomically accurate 3-D nose model. Particle deposition patterns were compared with and without electric forces for (a) the entire nostril release method (conventional delivery) and (b) the point-release method. (c) Significantly improved olfactory doses were achieved with electric guidance for both the conventional and point-release techniques. Electric-guided delivery increased the olfactory doses by approximately two orders of magnitude than without an electric field.

To further improve drug delivery to the olfactory mucosa, particles are released into a small point in the anterior nostril to minimize the filtration by the nasal valve and turbinate. With appropriate electric field strength, a majority (92%) of administered particles were dispensed to the olfactory region (red ellipse) that would have otherwise landed in the upper posterior nose in the absence of an electric field (**Figure 9b**, right vs. left). A careful study of the deposition distribution in the upper nose (green square, **Figure 9b**) shows that more aerosols are deposited on the turbinate wall (outer side) than on the septum (inner side). To minimize deposition in the turbinate, a lateral force is required to keep the aerosols from depositing onto the turbinate.

3.4. *In vitro* experiments of electric-guided olfactory delivery

3.4.1. Normal inhalation delivery

Particle deposition of charge particles was assessed in the realistic nose replicas. In order to generate a desirable electric field, two positive electrodes (25 and 100 V) were placed above the nose, and one electrode was placed below the nose as the ground. **Figure 10** compares deposition patterns of particles without and with electrostatic charges. For neutral particles, most inhaled particles deposited in the anterior nose while a small amount of particles reached the olfactory mucosa, which resembles the droplet deposition pattern visualized by Sar-Gel images (**Figure 5**). By contrast, significantly improved olfactory dosing was measured for charged particles under an external electric field (blue-dashed ellipse, **Figure 10b**). Meanwhile, filtration by the nasal vestibule and valve region was perceivably lower.

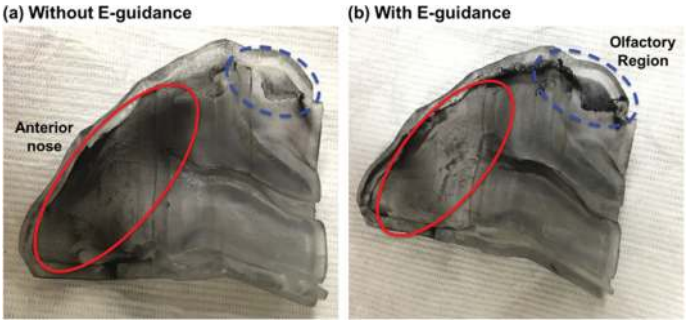

Figure 10. Particle deposition patterns in the 3-D nasal cast (a) without electric guidance versus (b) with electric guidance. Electric guidance of charged particles led to decreased deposition in the nasal valve region and noticeably enhanced deposition in the olfactory region.

3.4.2. Bi-directional delivery

The distribution of particle deposition using the bi-directional method is shown in **Figure 11**. High particle accumulations were observed in the upper nose of the right nasal passage, indicating there is an effective electric field guidance of charged particles to the olfactory region. It was also noted that particle deposition in the two passages was apparently different

http://dx.doi.org/ 10.5772/65858

(right panel, **Figure 11**). In the right passage, particle deposition was more uniformly distributed, and a large portion of particles appeared to be pulled toward the electrodes. By contrast, the majority of particles in the left passage deposited in the inferior nose while much fewer particles reached the upper nose, presumably due to the gravitational effect.

Figure 11. Deposition pattern in the right nasal passage and nasopharynx with the bi-directional delivery method. Appreciable deposition of particles was observed in the olfactory region. Because particles travel through the right and left passages in sequence, more particles were observed in the right passage than in the left passage.

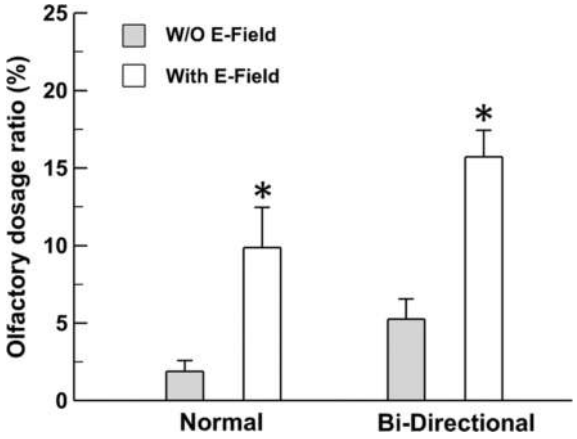

Figure 12. Comparison of the olfactory-to-nasal dosage ratio with and without electric guidance for the normal and bi-directional delivery strategies. *p-value < 0.05.

Figure 12 shows the comparison of the olfactory-to-nasal dosage ratio between the cases with and without the electric field guidance. The particle releasing time is 20 seconds, and the results are presented as the mean ± SD from five trials. With electric field guidance, significantly improved olfactory depositions were obtained for both delivery strategies, i.e., by a factor of 5 for the normal delivery and by a factor of 3 for the bi-directional delivery. The effect of the delivery method was also examined in the absence of an electric field; the olfactory dose using the bi-directional method was 2.8 times that under the normal method. However, with electric field guidance, the bi-directional olfactory dose was only 1.6 times the normal dose.

4. Discussion and conclusion

In this chapter, we presented a series of efforts in our lab aiming to improve the olfactory targeting of neurological medications. Both numerical and experimental tests were conducted to this aim by exploring various delivery strategies. Results of this study show that it is feasible to achieve clinically relevant olfactory doses using electric guidance of charged particles. All three protocols were demonstrated to give improved olfactory doses even though the improvement differs among the three. Compared to standard nasal devices, the point-release methods (vestibular and deep intubations) delivered approximately two order of magnitude higher doses to the olfactory region for both 150 nm and 1 μm particles. But even using the optimal delivery protocol (deep intubation), the olfactory dosage (1%) is still not adequate (~1%) to be clinically practical for the purpose of direct nose-to-brain drug delivery. In contrast, active control of drug particles using an externally applied electric field has been demonstrated to deliver much higher doses to target than the case without an electric field. An olfactory deposition fraction of 16% was measured with electric guidance under bi-directional breathing conditions.

The ability to dispense medications to the olfactory epithelium has tremendous superiority over convention inhalation devices in treating neurological diseases. A significantly enhanced olfactory dosing remits or eases the prevailing problem of too low olfactory doses. Second, reduced particle deposition in regions other than the olfactory region can minimize adverse side effects in those regions. Third, charged particles under the control of an external electric force will be are less dependent on respirations, making it suitable for seniors or subjects with comprised breathing capacities [52, 53]. The feature of robust delivery with electric guidance is especially appealing when the administration of medications requires long durations.

The electric delivery device is envisioned to have two major parts: a head-mounted nasal mask and a particle charging system. The nasal mask holds the electrodes and fixes the electrode relative to the patient head (**Figure 13a**). One example of the particle charging system is

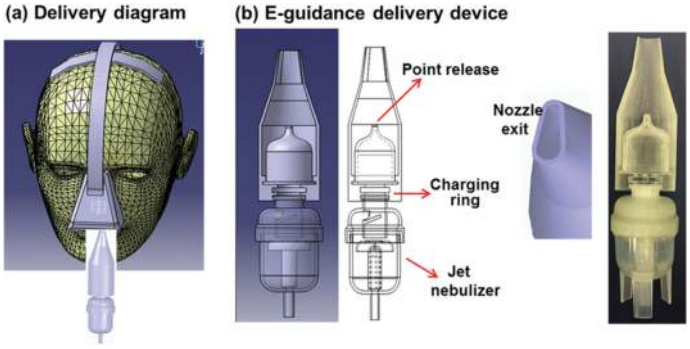

Figure 13. Electric-guidance olfactory delivery diagram and conceptual device designs. (a) A delivery system consists of two parts: a nose-mounted apparatus to generate desired electric field and a device to generate, charge, and point-release particles. (b) The conceptual delivery device uses a jet nebulizer and has an upright position.

http://dx.doi.org/ 10.5772/65858

illustrated in **Figure 13b** that contains a nebulizer, a charging ring, and a point-release nozzle. A prototype of this conceptual design was built using an Object30 Pro 3D printer (**Figure 13b**). An ideal design will generate small sized aerosols (<4 μm) at a slow speed and with high levels of electrostatic charges. Our preliminary test of this device, however, failed to produce such aerosols. Further testing and refinement are warranted to optimize the performance of this device.

Limitations of *in vitro* tests in this study include large particle size (30 μm), high exiting velocities of charge dry powders, large point-release area, and limited number of nasal models. Dry powders of 30 μm were selected because of the limited availability of dry powders satisfying both geometric and electrostatic requirements herein. Smaller aerosol particles are more sensitive to the guidance of electric forces and thus will lead to better doses in the olfactory region. A slow-moving particle will have longer residence time to respond to electric controls and is more likely to reach the target. In this study, the point-release catheter has a diameter of 4 mm and needs to be decreased to produce more site-specific doses. The nasal airway model was reconstructed from MRI images of one subject only and could not account intersubject variability. Future *in vitro* experiments and numerical simulations with more realistic scenarios are necessary to optimize the performance of electric-guidance delivery systems.

In conclusion, drug delivery of charged particles to the olfactory mucosa was assessed using both experiments and computations. Specific findings are as follows:

1. Complex nasal structure and no active control of particle motion in the nose are the two reasons lead to low doses in the olfactory region.
2. Conventional nasal devices, such as nasal drops, sprays, and nebulizers, fail to dispense clinically significant doses to the olfactory region.
3. The concomitant use of particle point release and electric field guidance can significantly enhance olfactory doses. With appropriate electric field and particle properties, a dose enhancement of two orders of magnitudes was predicted in both idealized 2-D and MRI-based 3-D nose models.
4. *In vitro* tests demonstrated a significantly higher olfactory dose using electric field guidance. There was a 5.2-fold increase for the normal delivery strategy and a 3.0-fold increase for the bi-directional strategy.
5. Future studies to refine the aerosol generation, charging, releasing, and guidance systems are warranted to further enhance the olfactory delivery.

Acknowledgements

Jun Lu at Central Michigan University, Linlin Zhao at Rutgers University, and Biwei Cao at Georgetown University are gratefully acknowledged for helpful discussions and for reviewing the manuscript.

Author details

Jinxiang Xi[1*] and Xiuhua April Si[2]

*Address all correspondence to: xi1j@cmich.edu

1 School of Engineering and Technology, Central Michigan University, Mount Pleasant, MI, USA

2 Department of Mechanical Engineering, California Baptist University, Riverside, CA, USA

References

[1] Bagger M, Bechgaard E. A microdialysis model to examine nasal drug delivery and olfactory absorption in rats using lidocaine hydrochloride as a model drug. Int. J. Pharm. 2004; 269: 311–322. doi: 10.1016/j.ijphann.2003.09.017

[2] Misra A, Kher G. Drug delivery systems from nose to brain. Curr. Pharm. Biotechnol. 2012; 13: 2355–2379. doi: 10.2174/138920112803341752

[3] Mistry A, Stolnik S, Illum L. Nanoparticles for direct nose-to-brain delivery of drugs. Int. J. Pharm. 2009; 379: 146–157. doi: 10.1016/j.ijpharm.2009.06.019

[4] Alam S, Khan ZI, Mustafa G, Kumar M, Islam F, Bhatnagar A, et al. Development and evaluation of thymoquinone-encapsulated chitosan nanoparticles for nose-to-brain targeting: a pharmacoscintigraphic study. Int. J. Nanomed. 2012; 7: 5705–5718. doi: 10.2147/ijn.s35329

[5] Shi H, Kleinstreuer C, Zhang Z. Laminar airflow and nanoparticle or vapor deposition in a human nasal cavity model. J. Biomech. Eng. 2006; 128: 697–706. doi: 10.1115/1.2244574

[6] Si X, Xi J, Kim J, Zhou Y, Zhong H. Modeling of release position and ventilation effects on olfactory aerosol drug delivery. Respir. Physiol. Neurobiol. 2013; 186: 22–32. doi: 10.1016/j.resp.2012.12.005

[7] Si X, Xi J, Kim J. Effect of laryngopharyngeal anatomy on expiratory airflow and submicrometer particle deposition in human extrathoracic airways. Open J. Fluid D. 2013; 3: 286–301. doi: 10.4236/ojfd.2013.34036

[8] Xi J, Longest PW. Numerical predictions of submicrometer aerosol deposition in the nasal cavity using a novel drift flux approach. Int. J. Heat Mass Transf. 2008; 51: 5562–5577. doi: 10.1016/j.ijheatmasstransfer.2008.04.037

[9] Illum L. Nasal drug delivery: new developments and strategies. Drug Discov. Today. 2002; 7: 1184–1189. doi: 10.1016/s1359-6446(02)02529-1

http://dx.doi.org/ 10.5772/65858

[10] El Taoum KK, Xi J, Kim JW, Berlinski A. In vitro evaluation of aerosols delivered via the nasal route. Respir. Care. 2015; 60: 1015–1025. doi: 10.4187/respcare.03606

[11] Wang J, Bentz J, Anderson R. Nasal device for delivery to the olfactory region. US 20070119451 A1. 2007.

[12] Gizurarson S. Method for administration of active substances to the olfactory region. Patents CA 2298596. 2003.

[13] Hoekman JD, Ho RJY. Effects of localized hydrophilic mannitol and hydrophobic nelfinavir administration targeted to olfactory epithelium on brain distribution. AAPS Pharmscitech. 2011; 12: 534–543. doi: 10.1208/s12249-011-9614-1

[14] Corley RA, Kabilan S, Kuprat AP, Carson JP, Minard KR, Jacob RE, et al. Comparative computational modeling of airflows and vapor dosimetry in the respiratory tracts of rat, monkey, and human. Toxicol. Sci. 2012; 128: 500–516. doi: 10.1093/toxsci/kfs168

[15] Xi J, Kim J, Si XA, Corley RA, Zhou Y. Modeling of inertial depositions in scaled models of rat and human nasal airways: towards in vitro regional dosimetry in small animals. J. Aerosol Sci. 2015; 99: 78–93. doi: 10.1016/j.jaerosci.2016.01.013

[16] Wilson IB. The deposition of charged particles in tubes, with reference to the retention of therapeutic aerosols in the human lung. J. Colloid Sci. 1947; 2: 271–276. doi: 10.1016/0095-8522(47)90028-7

[17] Bailey AG, Hashish AH, Williams TJ. Drug delivery by inhalation of charged particles. J. Electrostat. 1998; 44: 3–10. doi: 10.1016/S0304-3886(98)00017-5

[18] Wong J, Chan HK, Kwok PC. Electrostatics in pharmaceutical aerosols for inhalation. Ther. Deliv. 2013; 4: 981–1002. doi: 10.4155/tde.13.70

[19] Yu CP. Theories of electrostatic lung deposition of inhaled aerosols. Ann. Occup. Hyg. 1985; 29: 219–227. doi: 10.1093/annhyg/29.2.219

[20] Ferin J, Mercer TT, Leach LJ. The effect of aerosol charge on the deposition and clearance of TiO2 particles in rats. Environ. Res. 1983; 31: 148–151. doi: 10.1016/0013-9351(83)90071-3

[21] Ali M, Reddy RN, Mazumder MK. Electrostatic charge effect on respirable aerosol particle deposition in a cadaver based throat cast replica. J. Electrostat. 2008; 66: 401–406. doi: 10.1016/j.elstat.2008.02.005

[22] Scheuch G, Gebhart J, Roth C. Uptake of electrical charges in the human respiratory tract during exposure to air loaded with negative ions. J. Aerosol Sci. 1990; 21: S439–S442. doi: 10.1016/0021-8502(90)90275-3

[23] Azhdarzadeh M, Olfert JS, Vehring R, Finlay WH. Effect of electrostatic charge on oral-extrathoracic deposition for uniformly charged monodisperse aerosols. J. Aerosol Sci. 2014; 68: 38–45. doi: 10.1016/j.jaerosci.2013.11.002

[24] Xi J, Si X, Longest W. Electrostatic charge effects on pharmaceutical aerosol deposition in human nasal-laryngeal airways. Pharmaceutics. 2014; 6: 26–35. doi: 10.3390/pharmaceutics6010026

[25] Xi J, Si XA, Gaide R. Electrophoretic particle guidance significantly enhances olfactory drug delivery: a easibility study. PLoS ONE. 2014; 9: e86593. doi: 10.1371/journal.pone.0086593

[26] Melandri C, Tarroni G, Prodi V, De Zaiacomo T, Formignani M, Lombardi CC. Deposition of charged particles in the human airways. J. Aerosol Sci. 1983; 14: 657–669. doi: 10.1016/0021-8502(83)90070-8

[27] Hashish AH, Bailey AG, Williams TJ. Selective deposition of pulsed charged aerosols in the human lung. J. Aerosol Med. 1994; 7: 167–171. doi: 10.1089/jam.1994.7.167

[28] Ali M. Engineered aerosol medicine and drug delivery methods for optimal respiratory therapy. Respir. Care. 2014; 59: 1608–1610. doi: 10.4187/respcare.03634

[29] Balachandran W, Machowski W, Gaura E, Hudson C. Control of drug aerosol in human airways using electrostatic forces. J. Electrostat. 1997; 40: 579–584. doi: 10.1016/S0304-3886(97)00106-X

[30] Djupesland PG, Skretting A, Winderen M, Holand T. Bi-directional nasal delivery of aerosols can prevent lung deposition. J. Aerosol Med. Pulm. Drug Deliv. 2004; 17: 249–259. doi: 10.1089/0894268042176355

[31] Luthringer R, Djupesland PG, Sheldrake CD, Flint A, Boeijinga P, Danjou P, et al. Rapid absorption of sumatriptan powder and effects on glyceryl trinitrate model of headache following intranasal delivery using a novel bi-directional device. J. Pharm. Pharmacol. 2009; 61: 1219–1228. doi: 10.1211/jpp/61.09.0012

[32] Djupesland PG, Docekal P, Czech Migraine Investigators G. Intranasal sumatriptan powder delivered by a novel breath-actuated bi-directional device for the acute treatment of migraine: a randomised, placebo-controlled study. Cephalalgia. 2010; 30: 933–942. doi: 10.1177/0333102409359314

[33] Si X, Xi J. Modeling and simulations of olfactory drug delivery with passive and active controls of nasally inhaled pharmaceutical aerosols. J. Vis. Exp. 2016. 111:e53902. doi: 10.3791/53902

[34] Xi J, Longest PW, Martonen TB. Effects of the laryngeal jet on nano- and microparticle transport and deposition in an approximate model of the upper tracheobronchial airways. J. Appl. Physilo. 2008; 104: 1761–1777. doi: 10.1152/japplphysiol.01233.2007

[35] Xi J, Longest PW. Effects of oral airway geometry characteristics on the diffusional deposition of inhaled nanoparticles. J. Biomech. Eng. Trans. ASME. 2008; 130: 011008. doi: 10.011008.1115/1.2838039

http://dx.doi.org/ 10.5772/65858

[36] Xi J, Longest PW. Transport and deposition of micro-aerosols in realistic and simplified models of the oral airway. Ann. Biomed. Eng. 2007; 35: 560–581. doi: 10.1007/s10439-006-9245-y

[37] Xi J, Longest PW. Evaluation of a drift flux model for simulating submicrometer aerosol dynamics in human upper tracheobronchial airways. Ann. Biomed. Eng. 2008; 36: 1714–1734. doi: 10.1007/s10439-008-9552-6

[38] Longest PW, Vinchurkar S. Validating CFD predictions of respiratory aerosol deposition: effects of upstream transition and turbulence. J. Biomech. 2007; 40: 305–316. doi: 10.1016/j.jbiomech.2006.01.006

[39] Wilcox DC. Turbulence Modeling for CFD. 3rd ed. California: DCW Industries, Inc. 2006.

[40] Hinds WC. Aerosol Technology: Properties, Behavior, and Measurement of Airborne Particles. New York: John Wiley and Sons. 1999.

[41] Morsi SA, Alexander AJ. An investigation of particle trajectories in two-phase flow systems. J. Fluid Mech. 1972; 55: 193–208. doi: 10.1017/S0022112072001806

[42] Xi J, Longest PW. Characterization of submicrometer aerosol deposition in extrathoracic airways during nasal exhalation. Aerosol Sci. Technol. 2009; 43: 808–827. doi: 10.1007/s10439-008-9552-6

[43] Matida EA, Finlay WH, Grgic LB. Improved numerical simulation of aerosol deposition in an idealized mouth-throat. J. Aerosol Sci. 2004; 35: 1–19. doi: 10.1016/S0021-8502(03)00381-1

[44] Ribeiro P, Si X Section 2: Electric and Magnetic Circuit. In: Beaty HW, Fink DG, editors. Standard Handbook for Electrical Engineering. 16 ed: McGraw Hill, New York. 2012. pp. 2.1-2.58.

[45] Longest PW, Xi J. Effectiveness of direct Lagrangian tracking models for simulating nanoparticle deposition in the upper airways. Aerosol Sci. Technol. 2007; 41: 380–397. doi: 10.1080/02786820701203223

[46] Cheng YS, Su YF, Yeh HC, Swift DL. Deposition of thoron progeny in human head airways. Aerosol Sci. Technol. 1993; 18: 359–375. doi: 10.1080/02786829308959610

[47] Cheng KH, Cheng YS, Yeh HC, Swift DL. Deposition of ultrafine aerosols in the head airways during natural breathing and during simulated breath-holding using replicate human upper airway casts. Aerosol Sci. Technol. 1995; 23: 465–474. doi: 10.1080/02786829508965329

[48] Laube BL. Devices for aerosol delivery to treat sinusitis. J. Aerosol Med. 2007; 20: S5–S18. doi: 10.1089/jam.2007.0569

[49] Geller DE. Comparing clinical features of the nebulizer, metered-dose inhaler, and dry powder inhaler. Respir. Care. 2005; 50: 1313–1322.

[50] Covert D, Wiedensohler A, Russell L. Particle charging and transmission efficiencies of aerosol charge neutralizers. Aerosol Sci. Technol. 1997; 27: 206–214. doi: 10.1080/02786829708965467

[51] Zeng Y, von Klitzing R. Scaling of layer spacing of charged particles under slit-pore confinement: an effect of concentration or of effective particle diameter? J. Phys. Condens. Matter. 2012; 24: 464125. doi: 10.1088/0953-8984/24/46/464125

[52] Dhand R. Aerosol therapy in patients receiving noninvasive positive pressure ventilation. J. Aerosol Med. Pulm. Drug Deliv. 2012; 25: 63–78. doi: 10.1089/jamp.2011.0929

[53] Willis LD, Berlinski A. Survey of aerosol delivery techniques to spontaneously breathing tracheostomized children. Respir. Care. 2012; 57: 1234–1241. doi: 10.4187/respcare.01518